

Dear author,

Please note that changes made in the online proofing system will be added to the article before publication but are not reflected in this PDF.

We also ask that this file not be used for submitting corrections.



Contents lists available at ScienceDirect

Journal of Theoretical Biology

journal homepage: www.elsevier.com/locate/jtbi

Morphological and genetic characterisation of the root system architecture of selected barley recombinant chromosome substitution lines using an integrated phenotyping approach

C. De La Fuente Canto^{a,b,1}, D.I. Kalogiros^{a,c,1,2}, M. Ptashnyk^c, T.S. George^a, R. Waugh^a, A.G. Bengough^a, J. Russell^a, L.X. Dupuy^{a,*}

^aThe James Hutton Institute, Invergowrie, Dundee DD2 5DA, United Kingdom

^bSchool of Life Sciences, University of Dundee, Dundee DD2 1PP, United Kingdom

^cSchool of Science and Engineering, University of Dundee, Dundee DD2 1PP, United Kingdom

ARTICLE INFO

Article history:

Received 17 February 2017

Revised 12 March 2018

Accepted 13 March 2018

Available online xxx

Keywords:

Rootphenotyping

QTL

Barley

RCSL

Growth parameters

Computer assisted breeding

ABSTRACT

Discoveries on the genetics of resource acquisition efficiency are limited by the ability to measure plant roots in sufficient number and adequate genotypic variability. This paper presents a root phenotyping study that explores ways to combine live imaging and computer algorithms for model-based extraction of root growth parameters. The study is based on a subset of barley Recombinant Chromosome Substitution Lines (RCSLs) and a combinatorial approach was designed for fast identification of the regions of the genome that contribute the most to variations in root system architecture (RSA). Results showed there was a strong genotypic variation in root growth parameters within the set of genotypes studied. The chromosomal regions associated with primary root growth differed from the regions of the genome associated with changes in lateral root growth. The concepts presented here are discussed in the context of identifying root QTL and its potential to assist breeding for novel crops with improved root systems.

© 2018 Elsevier Ltd. All rights reserved.

1 Introduction

Profitability in modern agriculture relies heavily on the supply of water and fertiliser to maximise crop yield (Boserup, 2005). The current agro-economic model is now under increased scrutiny not only because of the damage it causes to the environment (Secchi et al., 2007), but also because of its possible vulnerability to climate changes (Letter et al., 2003) and the increasing cost and scarcity of some of the mineral compounds used in fertilisers (White et al., 2012). Reducing the dependency of modern agriculture on water and fertilisers is a major undertaking, and it has been proposed that breeding programs should now focus on the development of crop varieties that are more efficient at capturing the soil resources (Lynch, 2011).

To date, the genetic improvement of crops for improved resource acquisition efficiency has proved challenging. A plant acquires water and mineral elements from the soil through a sys-

tem of interconnected roots, the arrangement of which we refer to as the Root System Architecture (RSA). The RSA is a complex object for breeders and geneticists to comprehend and utilize. The length and topological arrangement of roots within the RSA is dynamic because growth and lifetime of individual roots is controlled by a combination of developmental, physiological and environmental signals perceived by the plant (Bingham et al., 2010; Forde and Lorenzo, 2001; Wilkinson and Davies, 2002). The development of RSAs is also very stochastic (Forde, 2009) and statistical characterization of root traits and growth parameters usually requires large replication numbers (Adu et al., 2014), observations in soil are destructive and labour intensive (do Rosario et al., 2000), and *in vivo* measurement techniques are partial (Nagel et al., 2012). Some progress has been achieved in the understanding of genetic control of RSA and its potential for breeding. For example recently, a QTL controlling root growth angle in rice, Deeper Rooting 1 (DRO1), has been characterised and cloned (Arai-Sanoh et al., 2014; Uga et al., 2013). Nevertheless, major constraints for genetic studies in RSA persist. Because root traits are greatly affected by the environment, their heritabilities in many cases are low compared to shoot traits (Courtois et al., 2009). Although genotypic variability is found for root traits in controlled conditions, and QTLs have been identified, very few have been translated and used routinely in breeding (de Dorlodot et al., 2007; Sandhu and Kumar, 2017).

* Corresponding author.

E-mail address: lionel.dupuy@hutton.ac.uk (L.X. Dupuy).

¹ These authors contributed equally to this study and are both considered as primary author.

² Current address: School of Mathematical Sciences, University of Nottingham, Nottingham, NG7 2RD, United Kingdom.

List of symbols and notations*Growth model*

x,y	Spatial coordinates (cm)
α	Root angle
t	time (d)
e	Elongation rate (cm·d ⁻¹)
b_r	Branching rate (d ⁻¹)
b_a	Branching angle
g	Gravitropic rate (d ⁻¹)
n	Total root number
l	Total root length (cm)
ρ_a	Root tip density (cm ⁻²)
ρ_l	Root length density (cm ⁻¹)
T	Time delay for lateral root initiation (d)
$\hat{}$	Direct estimate of a model parameter on data
$()$	Number in superscript and in parentheses indicate the root branching order

Genetic analysis

G^i	genetic make-up of the i th genotype
g_k^i	value of the k th introgression of the i th genotype. The value is 0 if the k th marker is that of the elite line and 1 if the marker is that of the exotic line.
φ^i	phenotype of the i th genotype represented as a scalar value, for example a root growth parameter
b_k	the genetic effect of the k th introgression
$D_k^{1,2}$	positive contribution to the score of the k th introgression determined from two subgroups of genotypes U_1 and U_2
E_k	negative contribution to the score of the k th introgression
δ_k^{12}	genetic difference factor that indicates when two subgroups of genotypes (U_1 and U_2) segregates at loci k
γ_k^r	genetic difference factor that indicates when a subgroup of genotype (U_r) has variation at loci k

25 QTLs should generally be validated in field conditions before using a marker assisted selection (MAS, Comas et al., 2013) but root traits measured *in vivo* are not always directly related to field performance. Hence, root QTL studies face limitations that need to be overcome through improved approaches able to dissect the genetic control of relevant RSA parameters for the development of more efficient crops.

26 There is great hope that technological development in root phenotyping systems could overcome some of these challenges. Traditionally, root phenotyping is achieved in the field using either soil coring or shovelomics. Soil columns are extracted from the field, roots contained in the soil columns are washed, and usually image analysis software is used to measure total root length in the sample (Watt et al., 2005). More recent shovelomics methodology relies on field measurement of the crown roots of the plant to describe parameters such as root gravitropism (Trachsel et al., 2011). These methods provide root data grown in their natural environment, but the measurements are destructive and time consuming. Non-destructive methods are a preferable approach to study roots (Downie et al., 2015). Mini-rhizotron tubes can be placed in the soil to observe roots *in situ* in undisturbed soils (Cai et al., 2016; Rewald and Ephrath, 2012); Laboratory-based rhizotron boxes allow part of the root system to be observed through glass windows (Nagel et al., 2012) with monitoring of root growth for long periods of time and image acquisition can be automated; X-ray computed tomography allows *in situ* imaging of soil cores of a range of size (Mooney et al., 2012), and various artificial media systems for

phenotyping are being developed (Clark et al., 2011; Downie et al., 2012; Topp et al., 2013).

27 Techniques to analyse the data produced by phenotyping systems are not advancing at a comparable rate. What appears to be a limiting factor is the ability to process data, derive quantitative information on the growth and developmental processes of plant roots and understand how these are genetically controlled. In this paper, we propose a new framework where processing of phenotypic data is tailored to the genetic material, here a set of barley Recombinant Chromosome Substitution Lines (RCSLs, Matus et al., 2003). We produced data using germination paper phenotyping system commonly used in the community (Gioia et al., 2017; Le Marié et al., 2014; Thomas et al., 2016), and developed mathematical modelling techniques to obtain chromosomal regions that are related to changes in the dynamic root growth parameters.

2. Material and methods*2.1. Plant material*

28 Five barley genotypes were chosen from a set of Recombinant Chromosome Substitution Lines (RCSLs, Fig. 1). The RCSLs were derived from an initial cross between a cultivated parent (cv. Harrington) and a naturally drought tolerant wild donor from the Fertile Crescent as described previously (Matus et al., 2003). Selection of the sub-set of genotypes was based on a previous assessment of the impact of drought on yield across two growing seasons during field trials (De La Fuente Canto et al, unpublished). Contrasting lines were selected: OSU044 and OSU048 showed a poor to moderate but stable yield across water treatments (stable RCSLs); OSU144 and OSU052 produced large yield potential in favourable conditions, but under drought their yield was significantly reduced (sensitive RCSLs); and finally, cv Harrington was chosen as control elite variety for the RCSLs and OSU060 as a line whose performance was intermediate and similar to the performance of cv. Harrington.

2.2. Experimental system

29 Plants were grown in a controlled environment in a 2D pouch and wick system (Hund et al., 2009; Liao et al., 2001). To avoid contamination during experiments, seeds with uniform size were surface sterilized by a vapour-phase sterilisation method using 100 ml sodium hypochlorite 4.5% and 5 ml concentrated HCl. The seeds were placed in opened Falcon tubes and treated for an hour with chlorine fumes inside a desiccator jar placed in a fume hood. Sterilised seeds were sown on 10 × 10 cm germination paper (Anchor Paper, St. Paul, MN, USA) moistened with sterile distilled water, placed in Petri dishes and maintained vertically in a Qualicool™ cooled incubator for two days at 20 °C with no light. The equipment used for the experiments, e.g. buckets, plates and acetate sheets, was thoroughly washed first in bleach and subsequently in ethanol. Three days after sowing (DAS), seedlings of similar size were transferred to large sheets of germination paper (29.7 × 52 cm) pre-soaked with the nutrient solution, described below. Seedlings were held on the germination paper between an A3 size clear-Perspex plate and a 240 μm thick acetate sheet.

30 Each germinated seed was placed in a slit at the top of the germination paper and glued to the plate with a drop of diluted Solvite wallpaper paste (Henkel Limited, Winsford Cheshire, UK). The germination paper was placed between a plate and an acetate sheet and held with two foldback clips attached on the sides and a clip hanger at the top. Each sample was then wrapped in aluminium foil to protect the roots from light and suspended into

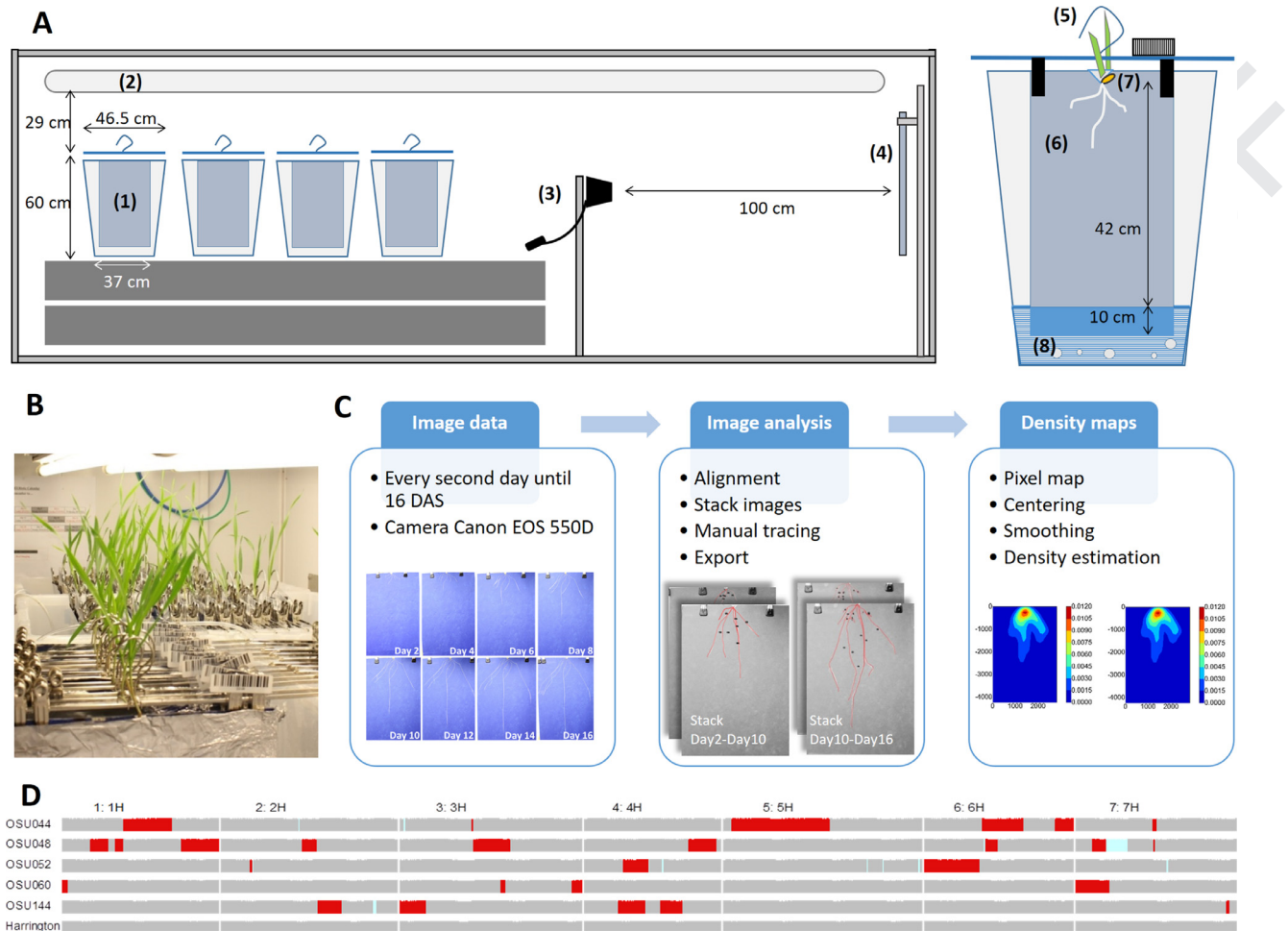


Fig. 1. The root phenotyping study. A) Diagram of the pouch-and-wick experimental setup used to grow barley seedlings under controlled conditions. (1) Each bucket contained two experimental replicates (12 seedlings, one per plate). (2) Lighting consisted of fluorescent tube light placed at 29 cm above the buckets and (3) a Canon EOS 550D camera was used for image acquisition. The camera was placed on a tripod with a remote shutter-release attached. (4) An artists' easel was used to hold the samples at a reference position and (5) the clip hangers used to hold the samples on the easel were fitted with a barcode. (6) Roots grew on A3 size clear-Perspex plate and acetate sheet with blue germination paper in between. Each plate was wrapped in foil and (7) seedlings were attached in a slit on top of the germination paper. (8) The nutrient solution was aerated with a pneumatic pump and 10 cm of the germination paper was submerged in nutrient solution. B) Picture of the experiment in the growth room. C) Diagram of the data processing framework. The raw phenotyping data consisted of images taken every two days for 15 days after sowing. The images were analysed using a series of steps including registration for aligning data with a reference image, stacking, tracing and exporting the pixel ROI data to files. Pixel ROI data were then used to generate root density distribution maps for primary and lateral roots. This was done using kernel-based density distribution methods combined with a centering of the data with respect to the midpoint of the horizontal plane (position of the slit on the germination paper). D) Graphical representation of the genotypes of the 5 RCSLs used in the study and cv. Harrington. Dark red areas indicate the introgressions from the wild parent and light grey areas indicate the modern background. Missing marker data are indicated in light blue. Each chromosome is oriented with the short arm from the left. (For interpretation of the references to colour in this figure legend, the reader is referred to the web version of this article).

112 plastic boxes (60 cm × 68 cm × 46.5 cm) containing 30 L of nutri-
 113 ent solution into which only approximately 10 cm of the germina-
 114 tion paper was submerged (Fig. 1). The nutrient solution was con-
 115 stantly aerated with a pneumatic pump and changed every four
 116 days.

117 The same nutrient solution was used to soak the germina-
 118 tion paper and to fill in the plastic containers. The nutrient so-
 119 lution was prepared with deionized water and contained 300 mM
 120 NH₄Cl, 400 mM Ca(NO₃)₂, 400 mM KNO₃, 300 mM MgSO₄, 100 mM
 121 FeEDTA, 1 M KH₂PO₄, 6 mM MnCl₂, 23 mM H₃BO₃, 0.6 mM ZnCl₂,
 122 1.6 mM CuSO₄, 1 mM Na₂MoO₄, 1 mM CoCl₂. The pH was adjusted
 123 to 5.5 at the start of the experiment using NaOH and the nutri-
 124 ent solution was replaced every four days. Eight replicates of
 125 each genotype were distributed in four plastic boxes, two complete
 126 replicates per box. Plants were grown for 15 days in a growth room
 127 under a 16/8 h day/night cycle at a constant temperature of 15 °C
 128 and 60% relative humidity approximately. Average light intensity
 129 during the day hours was 80 μmol m⁻² s⁻¹ at plant height.

2.3. Phenotyping system 130

2.3.1. Image acquisition 131

132 Pictures of each plate were taken every two days from day 2 to
 133 day 16 of the experiment with a Canon EOS 550D camera fixed on
 134 a tripod set on autofocus mode at a distance of 1 m from the ger-
 135 mination paper. The plate was hung in an easel with a 1 m working
 136 distance. The aluminium foil and acetate sheet were removed for
 137 taking pictures and, before putting them back, the germination pa-
 138 per was sprayed with approximately 1 ml of the nutrient solution
 139 to ensure a homogeneous diffusion of the nutrients in the root sys-
 140 tem growing media and avoid mineral deficiency towards the end
 141 of the experiment.

2.3.2. Harvest 142

143 After the last image, 18 day-old seedlings were removed
 144 from the plates. Shoots were excised from the roots and fresh
 145 weight of the shoots was recorded. Roots were detached from the

germination paper and stored at room temperature in 50% ethanol until scanning. A reference picture of the final root system was acquired in high resolution (400dpi) using an Epson Expression 10,000XL professional DIN A3 scanner (Seiko Epson Corporation, Japan). Analysis of scanner images were performed with WinRHIZO (Regent Instruments, Quebec, Canada) to collect data on average root diameter and total root length at harvest. Shoots and roots were dried at 60 °C for 72 h before determining dry weight (DW).

2.3.3. Image processing

Image data were analysed through manual tracing of individual root trajectory using a liyama ProLite T2735MSC touch screen and Fiji software (Schindelin et al., 2012). Raw images were first transformed into 8-bit grayscale images. For each genotype, the elongation rate of seminal and lateral roots as well as the branching rate of seminal roots were analysed on two time-steps, from day 2 to day 10 and from day 10 to day 16 of growth. Tracing was obtained using the freehand tool for several reasons. Automated tracing tool requires manual adjustment due to variation in the background or difficulty to detect small roots (Leitner et al., 2014; Lobet et al., 2011; Pound et al., 2013), and the majority of lateral roots were too short to gain benefit from automation. Also, the analysis does not require topology but just length distribution and the time gained by automated tracing is offset by the requirement to connect seminal roots with laterals. ROI (Region Of Interest) files produced for seminal and lateral roots of all the replicates for each genotype were then processed by a custom macro so that the pixel coordinates of all roots in the images were exported in text files.

Tracking of individual roots in coarse time lapse automatically is not easy, and often not possible when roots are grown in soil. We propose, instead, to determine growth parameters directly from changes in total root length and total root numbers during the course of the experiments. Such estimates can be obtained because in the absence of mortality there is a direct relationship between elongation rate, branching rate, total number of roots and total root length. The relationship was proposed by Hackett and Rose (1972) and it can be transformed to derive root growth parameters:

$$\begin{aligned} e^{(0)}(t) &= \frac{l^{(0)}(t+dt) - l^{(0)}(t)}{n^{(0)}dt} \\ b_r^{(0)}(t) &= \frac{n^{(1)}(t+dt) - n^{(1)}(t)}{dt - T} \\ e^{(1)}(t) &= \frac{2l^{(1)}(t+dt) - l^{(1)}(t)}{n^{(0)}b_r^{(0)}(dt - T)^2}. \end{aligned} \quad (1)$$

Here, $e^{(0)}(t)$ and $e^{(1)}(t)$ (cm d⁻¹) are the elongation rate for, respectively, the seminal and lateral roots and $b_r^{(0)}(t)$ (d⁻¹) is the branching rate of lateral roots. The parameter dt indicates the duration of the examined growth interval of 8 days (day 2 to day 10) and 6 days (day 10 to day 16) respectively, while $l^{(0)}(t)$ (cm) and $l^{(1)}(t)$ (cm) are the total seminal and lateral root length at time t , respectively. The number of seminal roots is denoted by $n^{(0)}(t)$, the total number of laterals is denoted by $n^{(1)}(t)$. Since the number of seminal roots for the replicates of each genotype increased with time, $n^{(0)}$ was taken as the mean number of seminal roots during a given time interval where growth parameters were determined. For lateral roots, there was a time delay between the emergence of the first appeared seminal and the emergence of lateral roots. The parameter T (d) is therefore the time it takes for lateral roots to emerge from the primary root. In this experiment, it applied only to the first time step (day 2 - day 10), since after 8 days, laterals had emerged from all primary roots. T was evaluated as the mean value of the time delay observed among the replicates of a single genotype.

The rate at which the angle of the root changes towards verticality (termed gravitropic rate) was determined using stacked images from day 2 and day 4. Images were first registered (alignment of the base of the root system) using the plugin Align Image by line ROI (Schindelin et al., 2012). Registration of images used the top and bottom of the slit as common feature to perform alignment across the different images of a given plant. Two types of angles were recorded for these images. First the angle of the root with the vertical axis (α) was measured at day 2 using the Straight Line ROI. In this setting, α is 0 when the root is vertical. Then, the change in angle ($d\alpha$) taking place for the same root between day 2 and day 4 was determined as the angle between the two segments of root (between day 2 and day 4) using Segmented Line ROI and angle measurement. Three randomly selected seminal roots of each plate were measured. The root gravitropic rate parameter ($g^{(0)}$) is defined as the relative decrease in vertical angle per unit time and it was determined for each genotype using the information gathered for a total of 24 seminal roots as follows:

$$g^{(0)}(t) = \frac{\alpha(t) - \alpha(t+dt)}{\alpha(t)dt} \quad (2)$$

where dt is equal to 2, since the change in angle was measured for an interval of 2 days.

2.3.4. Genetic analysis

A scoring system termed Combinatorial Quantitative Trait Loci (C-QTL) is proposed to visualise the effect of exotic introgressions on the root growth parameters measured during the experiments. The algorithm exploits the genomic structure of the introgressions and processes markers by blocks during the analysis. An algorithm is then designed to score each block of markers. The algorithm selects two groups of genotypes and considers blocks of markers that vary between and within the groups of genotypes and adds to or subtracts from the score based on phenotypic differences. The process is repeated for all possible groups of genotypes to provide an overall score for each block of markers.

Formally, the C-QTL score from the set of plants phenotypes φ^i is derived from the genetic composition G^i of a genotype. The genetic composition of the i th plant is defined as $G^i = \{g_1^i, g_2^i, \dots, g_n^i\}$ with $i \leq s$ (number of blocks), such that g_k^i takes the value 0 if the k th block of markers is that of the elite line and g_k^i takes the value of 1 if the k th block of markers is that of the exotic line. The i th genotype is also defined by its phenotype φ^i which is the quantitative trait corresponding to the genetic make up G^i . We therefore assume genotypes and phenotypes are related according to the following probabilistic model:

$$P(\varphi^i < x) = \int_{-\infty}^x N\left(x - a^i - \sum_{k \leq n} b_k g_k^i, \sigma\right) dx \quad (3)$$

where φ^i is considered to be normally distributed so that $N(x - a^i - \sum_{k \leq n} b_k g_k^i, \sigma)$ is the Gaussian function of mean $x - a^i - \sum_{k \leq n} b_k g_k^i$ and standard deviation σ . Here a^i is the mean trait value observed on the modern variety, b_k is the effect of the i th marker on the genotype, σ is the standard deviation of the residual, and N is the Gaussian distribution function. If two groups of distinct genotypes U_1 and U_2 are obtained, then variations between and within groups can be exploited to score each region of the genome using the following formula:

$$D_k^{1,2} = \delta_k^{1,2} \left(\frac{1}{n_1} \sum_{i \in U_1} \varphi^i - \frac{1}{n_2} \sum_{j \in U_2} \varphi^j \right), \quad (4)$$

$$E_k = \sqrt{\max_{r=1,2} \left(\frac{\gamma_k^r}{n_r} \left(\sum_{i \in U_r} \varphi^i - \varphi^r \right)^2 \right)} \quad (5)$$

256 where $\gamma_k^r = 1$ if there exists two genotypes P_i and P_j in U_r such
257 that $g_k^i \neq g_k^j$ and $\gamma_k^r = 0$ otherwise. E_k is therefore an estimate of
258 the standard error of the mean within groups of genotypes.

259 Since there are many possible groupings on which to carry out
260 such analysis, a logical and computationally efficient way to pro-
261 cess the entire dataset is to use a clustering algorithm to group
262 genotypes based on their similarity and to cumulate the indicators
263 D_k and E_k on the possible set of clusters identified. The following
264 formula is therefore obtained for scoring individual markers:

$$I_{C-QTL} = \left\{ \frac{1}{n_{clusters} - 1} \times \sum_{k=3}^{k \leq n_{clusters}} \left[\frac{1}{n_{clusters}^2 - n_{clusters}} \left(\sum_{i,j \leq n_{clusters}} D_k^{i,j} \right) - E_k \right] \right\}. \quad (6)$$

265 C-QTL analysis was run for all four root growth parameters:
266 the elongation rate of seminal root $e^{(0)}$, the elongation rate of lat-
267 eral roots $e^{(1)}$, the branching rate $b_r^{(0)}$ and the gravitropic rate $g^{(0)}$
268 (the rate at which the angle of the root changes towards vertical-
269 ity). The data were transformed so that the value of each of these
270 growth parameters had zero mean and variance equal to 1. Clusters
271 were created using the Agglomerative Clustering from the Scikit li-
272 brary (Pedregosa et al., 2011).

273 2.3.5. Description of the change of the root system over time using a 274 time-delay density based model

275 Direct estimation of root growth parameters from an experi-
276 mental dataset is often problematic. It requires tracking and meas-
277 uring the growth of single roots at different time points. It is
278 time consuming at best and not possible when partial observa-
279 tions are made, for example in rhizotron systems. The Hackett and
280 Rose (1972) approach allows direct estimation of growth param-
281 eters in bulk and remove the need for tracking individual roots,
282 but it lacks a true spatial formalism. It does not provide ways of
283 estimating parameters such as gravitropic rate, branching angle or
284 responses to spatial heterogeneity, and results of direct estimations
285 are sensitive to missing data (Kalogiros et al., 2016). Hence, we
286 propose a model that extends Hackett and Rose (1972) approach
287 to include the spatial distribution of roots. Because both space and
288 time are considered, the model was generalised into a set of par-
289 tial differential equations including both time and space derivatives
290 and also requiring more sophisticated numerical techniques to de-
291 rive the growth parameters.

292 The mathematical framework proposed to build on the work
293 presented in Kalogiros et al. (2016) where root systems were mod-
294 elled as a continuum and changes in the architecture of the root
295 system over time were mathematically described with time-delay
296 partial differential equations. The initial model was extended so
297 that it could be used to extract growth parameters from time-
298 lapse data. Modifications included time-varying growth parameters
299 to characterise the changes in growth patterns over time, enabling
300 the time delay in the emergence of lateral roots to be consistent
301 with the time-lapse data considered in order to facilitate the spa-
302 tial and temporal evolution of RSA.

303 Root density distributions are functions depending on the hor-
304 izontal distance (x), depth (y) and root angle (α), which was
305 defined with respect to the vertical axis. Therefore, at any point
306 (x, y, α) the number of root tips per unit volume changes accord-
307 ing to the main conservation equation:

$$\frac{\partial \rho_a^{(i)}}{\partial t} + \nabla \cdot \left(e^{(i)} \rho_a^{(i)} (\sin \alpha, \cos \alpha, -g^{(i)} \alpha) \right) = b^{(i)}, \quad \text{with } i \geq 0 \quad (7)$$

The index (i) describes the type of root so that seminal roots 308
are denoted with the index 0 and lateral roots are denoted with 309
the index 1. The root tip density is denoted by $\rho_a^{(i)}$ (cm^{-2}) and 310
 $\frac{\partial \rho_a^{(i)}}{\partial t}$ is the change with respect to time of the root tip den- 311
sity. The operator ∇ is the divergence with respect to the inde- 312
pendent variables x , y , α and $e^{(i)}(t)$ ($\text{cm } d^{-1}$), $g^{(i)}(t)$ (d^{-1}) and 313
 $b^{(i)}(t)$ ($\text{cm}^{-2} d^{-1}$) describe respectively the elongation rate, gravit- 314
ropic rate and the volumetric branching rate (termed also “branch- 315
ing rate” in the following sections) as functions of time. Since only 316
seminal roots emerged from the base of the root system during the 317
experiment, $b^{(0)} = 0$. For lateral roots, the branching rate is non 318
zero and is specified as 319

$$b^{(i)}(x, y, \alpha, t) = \frac{1}{2} b_r^{(i-1)} \left[\rho_a^{(i-1)}(x, y, \alpha + b_a^{(i)}, t - T^{(i)}) \right. \\ \left. + \rho_a^{(i-1)}(x, y, \alpha - b_a^{(i)}, t - T^{(i)}) \right], \quad \text{with } i \geq 1, \quad (8)$$

where $T^{(1)}$ (d) is the time delay observed before the emergence of 320
the first appeared 1st order lateral root, $b_r^{(i-1)}$ (d^{-1}) is the seminal 321
root branching rate and $b_a^{(i)}$ is the branching angle. In this setting, 322
the root length density distributions $\rho_l^{(0)}$ and $\rho_l^{(1)}$ are derived from 323
the root tip density distribution as $\int e^{(0)}(t) \rho_a^{(0)}$ and $\int e^{(1)}(t) \rho_a^{(1)}$, 324
respectively. Numerical solutions for Eqs. (7) and (8) were obtained 325
using an upwind finite volume solver with minmod flux limiters. 326

273 2.3.6. Spatial and temporal mapping of the root system architecture 274 using density functions

275 In the next stage, the root tracing data were transformed into 329
root length density so that model predictions could be compared 330
directly to experimental data. The lists of pixels describing root 331
trajectories (ROI) were first processed to extract lists of root seg- 332
ments, their spatial coordinates, the length of the segment and its 333
angle. Length density distribution functions were then determined 334
using a kernel-based density estimation method. The method fol- 335
lowed the principles of Kalogiros et al. (2016) but in this study, it 336
was applied to pixel data directly and at different times during the 337
experiment (day 2, day 10 and day 16). Kernel functions were fit- 338
ted on data by the adjustment of the band width k of the kernel 339
function. A Gaussian function was used to obtain smooth repre- 340
sentation of the densities and facilitate fitting of solutions of the 341
model to the data. The heterogeneity of the distribution of root 342
segments in space is a main challenge in order to achieve a good 343
fit, because the data point distribution is dense along a root and 344
sparse between roots. In this case, it is advantageous to consider 345
groups of segments belonging to a single root (V-fold grouping) 346
and apply cross validation to these groups of roots instead of sep- 347
arate random data points (Kalogiros et al., 2016). 348

349 In a time-lapse dataset, both the number of root segments and 350
the volume explored by roots increase with time. These two fac- 351
tors have an opposite effect on the optimal k , with a higher num- 352
ber of segments lowering k values and a larger explored volume 353
increasing k values. Overall, k values always increase because the 354
number of points increase linearly with time, but the explored vol- 355
ume increases more rapidly as a power function of time. In order 356
to simplify the analysis, we choose the largest optimal value of 357
 k which was always on the last day of growth. Hence, the band- 358
width k was first evaluated on the last day of the experiment (day 359
16) and the same value was used for estimating the root length 360
density for the other time points of the experiment. Finally, the 361
seminal root length density distribution maps on each day were

aligned with respect to the midpoint of the horizontal distance of the plane (Fig. 1; Step C).

2.3.7. Estimation of time-dependent model parameters from time-lapse data

The Hackett and Rose (1972) approach allows direct estimation of root growth parameters (Eq. 1) because the model can be inverted analytically to provide simple formula for growth parameters. This is not the case in general for fitting the currently presented model to experimental data. Instead, simulation algorithms must be used to find optimal parameters that best describe the series of experimental observations. With these stepwise algorithms (described formally below) the model is first initiated with the root density distribution at day 2 of the experiment. Subsequently, an error function must be defined to quantify the difference between observed and modelled root length density. A minimisation algorithm then provides the best set of parameters to move from the initial condition to the next step of the experiment. This procedure is repeated for the different growth increments recorded during the experiment.

Here, the length density was initiated directly using the kernel-based density estimation. Since it is not possible to distinguish between root tips and root bases from the tracings, the length density at day 2 was also used to determine the root tip density, as follows:

$$\rho_a^{(0)}(x, y, \alpha, 2) = n^{(0)} \frac{\hat{\rho}_l^{(0)}(x, y, \alpha, 2)}{\int \hat{\rho}_l^{(0)}(x, y, \alpha, 2) dx dy d\alpha} \quad (9)$$

with $\hat{\rho}_l^{(0)}$ denotes the root length density distribution function estimated using kernel-based methods from the experimental data made available on day 2. The same data were used to determine the initial value of the root length density at the beginning of the numerical simulation of the model. The optimal set of growth parameters was obtained using the following robust error function $E^{(i)}$:

$$E^{(i)} = \int_V \hat{\rho}_l^{(i)2} (\rho_l^{(i)} - \hat{\rho}_l^{(i)})^2 dx dy d\alpha + \left(\int_V (\rho_l^{(i)} - \hat{\rho}_l^{(i)}) dx dy d\alpha \right)^2 \quad (10)$$

The first integral term accounts for local differences between the observed $\hat{\rho}_l^{(i)}$ and predicted $\rho_l^{(i)}$ root length density. It is a modification of the mean square error that reduces the dependency of the error on areas of relatively low root length density in the spatial domain. The second term of the error accounts for the differences in the total root length density. The Nelder–Mead optimisation algorithm was used to obtain the parameter values $e^{(0)}$ and $g^{(0)}$. Lateral root growth parameters $b_r^{(0)}$ and $e^{(1)}$ were obtained in a second stage.

Model fitting was carried out stepwise, with each experimental time increment treated as a distinct optimisation sub-problem. Both the model parameters and the root densities (root length and root tip density) were initiated from those obtained from the previous sub-problem. To insure stability of the simulations, the time increment of simulations was fixed to the smallest admissible increment for all the sub-problems determined from the Courant–Friedrichs–Lewy condition. To maintain a constant grid size, the bandwidth k of the density estimation was determined on the last time-step of the experiment (largest k value for each genotype).

First, the parameter extraction pipeline was benchmarked on simulated data for which growth parameters were known. The model used to establish the benchmark consisted of Eqs. (7) and (8), for which the elongation rate $e^{(0)}$ was either a linearly decreasing function of time or exponentially decreasing function of time and the branching rate $b_r^{(0)}$ increased exponentially with time. The

data generated by these models were used in the optimisation algorithm described above and the results were compared with the model parameters used to generate the target root length density function. In the second step, the optimisation algorithm was applied to the entire root tracing dataset (Fig. 2). For each time interval the Model Elasticity Value (MEV) of the error was determined as the percentage increase in the error induced by a 1% increase in each model parameter. Confidence intervals for model parameters were estimated using the V-fold bootstrap method proposed in Kalogiros et al. (2016).

2.3.8. Software for numerical simulations and statistical analysis

Numerical simulation of the model equations and parameter estimation was performed using the Python programming language (Python Software Foundation. Python Language Reference, version 2.7. Available at <http://www.python.org>). The algorithms were implemented in the Python SciPy library (<http://www.scipy.org/>) using a personal computer of 3.1 GHz CPU (Intel Core i5-2400 CPU @ 3.1 GHz) and 4 Gb RAM. We provide software and code for simulation and estimation of growth parameter from root tracing data under the BSD and GNU General Public License. The modules provided include a) the numerical algorithm for root simulation of root growth (Main.py), b) algorithms for estimation of length density mappings from experimental data (Roots_VFold_CrossValidation.py) and c) algorithms for the extraction of growth parameters from experimental data (Optimisation.py). All the programs can be downloaded at <http://archiroot.org.uk/tools/model-based-phenotyping.html>. Statistical analysis of the genotypic effects on root traits was performed using a two factorial mixed model considering the genotype, the time-step (day 2 to day 10, day 10 to day 16 of the experiment) and their interaction as fixed effects. The experimental replicate was considered as the random effect. Genstat 17th Edition (VSN International, UK) was used for this analysis.

3. Results and discussion

3.1. Integrated phenotyping and computational methods allow automated extraction of growth parameters

The phenotyping system based on germination paper was tailored for the observation of barley roots of up to 18 days-old and image acquisition using a DSLR camera. After fifteen days of growth, seminal roots fitted tightly within the boundaries of the A3 sized pouches, without touching any of the edges. Similar phenotyping systems have been successfully used in cereal crop plants such as maize (Hund et al., 2009), wheat (Atkinson et al., 2015) and brassica species (Adu et al., 2014; Thomas et al., 2016). The preparation of samples and room temperature during growth allowed good control of contamination from fungi and algae with no significant contamination observed after 18 days of growth. Elongation rate of seminal roots (approximately 1–2.5 cm d⁻¹) was similar to those measured in soil (Dupuy et al., 2010; Valentine et al., 2012), in hydroponics (Rose, 1983) or in gels (Shelden et al., 2013). Visual inspections of the plant showed vigorous growth and no signs of stress and mineral deficiencies. Other simple phenotyping systems have been used in the past e.g. gel chambers (Bengough et al., 2004), imaging at the surface of transparent cylinders (Kristensen and Thorup-Kristensen, 2004) or gel systems (Topp et al., 2013), but cost and the time for sample preparation in such systems is higher. Although the study focused on few selected genotypes, results showed the phenotypic pipeline is suitable to detect genotypic variations in rooting traits, and similar analyses could be carried out on larger number of genotypes simply by allowing for more pouches to be grown simultaneously during an

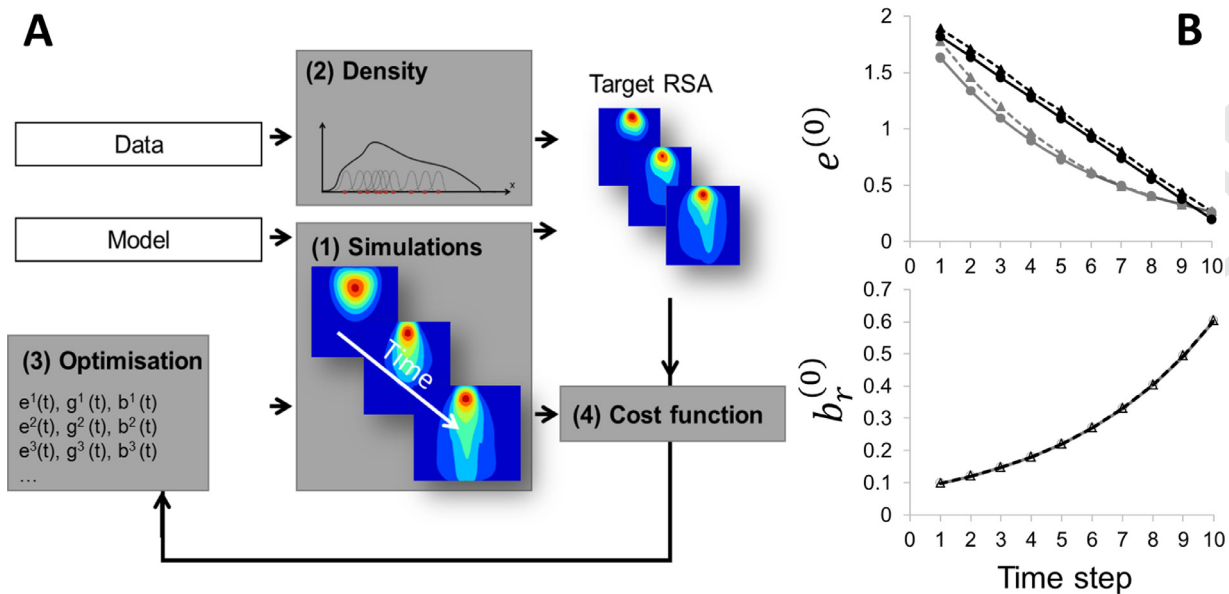


Fig. 2. A) Diagram of the optimisation process for automatic identification of growth parameters over time. The target root system architecture (RSA) at specific time points results from the available experimentally observed time-lapse data or artificial data (model-generated data with model parameters known). A target root length density distribution function is derived from simulations with user-defined time-varying parameters for each time step (1) so that it is feasible for the estimated model parameters to be directly compared with target parameters over time. When dealing with experimental data, root density estimation methods (2) are applied to obtain the target RSA. Then, the optimal time-dependent model parameters are determined by applying a minimisation algorithm (3) that proposes, at each time step, a set of new candidate model parameters. The new set of parameters is then used in a simulation and the results of this simulation are compared with the target root system using a cost function (4). The optimisation procedures (3 and 4) are iterated until a convergence criterion is met. The output seminal root distributions with the estimated optimal parameters at a specific time step are used as the initial condition for the evaluation of the optimal model parameters at the next time step. B) The quality of the fit obtained with the optimisation algorithm was tested on simulated data using time-varying elongation rate and branching rate. In the top figure, the imposed elongation rates (linearly or exponentially decreasing with time) are drawn using plain lines and those retrieved by the optimisation algorithms are drawn in dashed lines. Additionally, in the bottom figure, the imposed branching rate is drawn using plain lines and those retrieved by the algorithms using dashed lines.

479 experiment. This has been achieved in a recent study on Brassica
480 genotypes (Thomas et al., 2016).

481 Our approach to the analysis of root data included manual oper-
482 ations to handle the samples and analyse the images, with about
483 one minute required to trace an entire root system. However, Vari-
484 ous software and techniques are now being developed to automate
485 the analysis of root images. Robots are being used to acquire image
486 data automatically (Nagel et al., 2012) and root tracing algorithms
487 (Armengaud et al., 2009; Lobet et al., 2011; Pound et al., 2013) can
488 be used to obtain descriptions of the root system and its topology.
489 Recent developments made in computer vision also indicates there
490 is a great potential for new software to remove most manual inter-
491 ventions from image processing. Techniques could for example
492 combine root tip detection (Kumar et al., 2014) with optimal path
493 search (Pound et al., 2013), active contour (Makowski et al., 2002),
494 or tracking algorithms (Mairhofer et al., 2012). However, the de-
495 velopment of automated image analysis techniques may unleash
496 large quantity of complex root data for which there is currently
497 no method or strategy to process and analyse. In particular, it has
498 proved particularly difficult to derive meaningful growth param-
499 eters from root growth data when only parts of the root system
500 is visible (Dupuy et al., 2010; Garré et al., 2012). Research pre-
501 sented here shows that mathematical models of root systems pro-
502 vide a useful framework to perform such tasks, applicable on var-
503 ious plants and different types of experimental systems including
504 rhizotrons (Kalogiros et al., 2016).

505 3.2. Mathematical models allow accurate estimation of time varying 506 growth parameters

507 Optimisation techniques have been used for model calibra-
508 tion (Reddy and Pachepsky, 2001) to predict, for example, the

509 spread of roots through soil under different fertilisation regimes
510 (Heinen et al., 2003). The problem of extracting biologically mean-
511 ingful information from data is more challenging because models
512 can make accurate predictions including parameters with no bi-
513 ological significance. Recent attempts to solve this problem have
514 shown that root growth rates can be estimated accurately when
515 the root system is simple (Kalogiros et al., 2016), but when more
516 complex models are used the optimisation process is more chal-
517 lenging (Garré et al., 2012).

518 The difficulty of extending optimisation of model parameters to
519 time varying parameters and time lapse data is that parameters
520 of the numerical algorithm for model simulation such as grid size,
521 time increment or the size of the data buffer for simulation of de-
522 lays are dependent on both the duration of growth and the ob-
523 served root system through the bandwidth k of the kernel estima-
524 tor.

525 Assessment of the performance of our method was carried out
526 visually through comparison of the experimental root length den-
527 sity distributions with the predicted root length density distribu-
528 tions. (Fig. 3A and B). The growth parameters obtained on the ex-
529 perimental data were also compared with direct measurements
530 (Fig. 3C–E, Tables 1 and 2). Strong correlations were observed
531 between direct measurements of growth parameters and model
532 based estimations of those parameters. All correlations were sig-
533 nificant ($p < 0.001$). Model predictions were greater for the elonga-
534 tion of seminal roots. The elongation rate had a coefficient of vari-
535 ation varying between 5% and 20%, and there was little bias with
536 overestimation of the predictions by a factor of 1.03 (Fig. 3C). The
537 growth of lateral roots was more stochastic with a coefficient of
538 variation for the branching rate ranging between 9% and 94% and
539 for the elongation rate between 20% and 110%. This variability af-
540 fected considerably the predictions. The branching rate of lateral

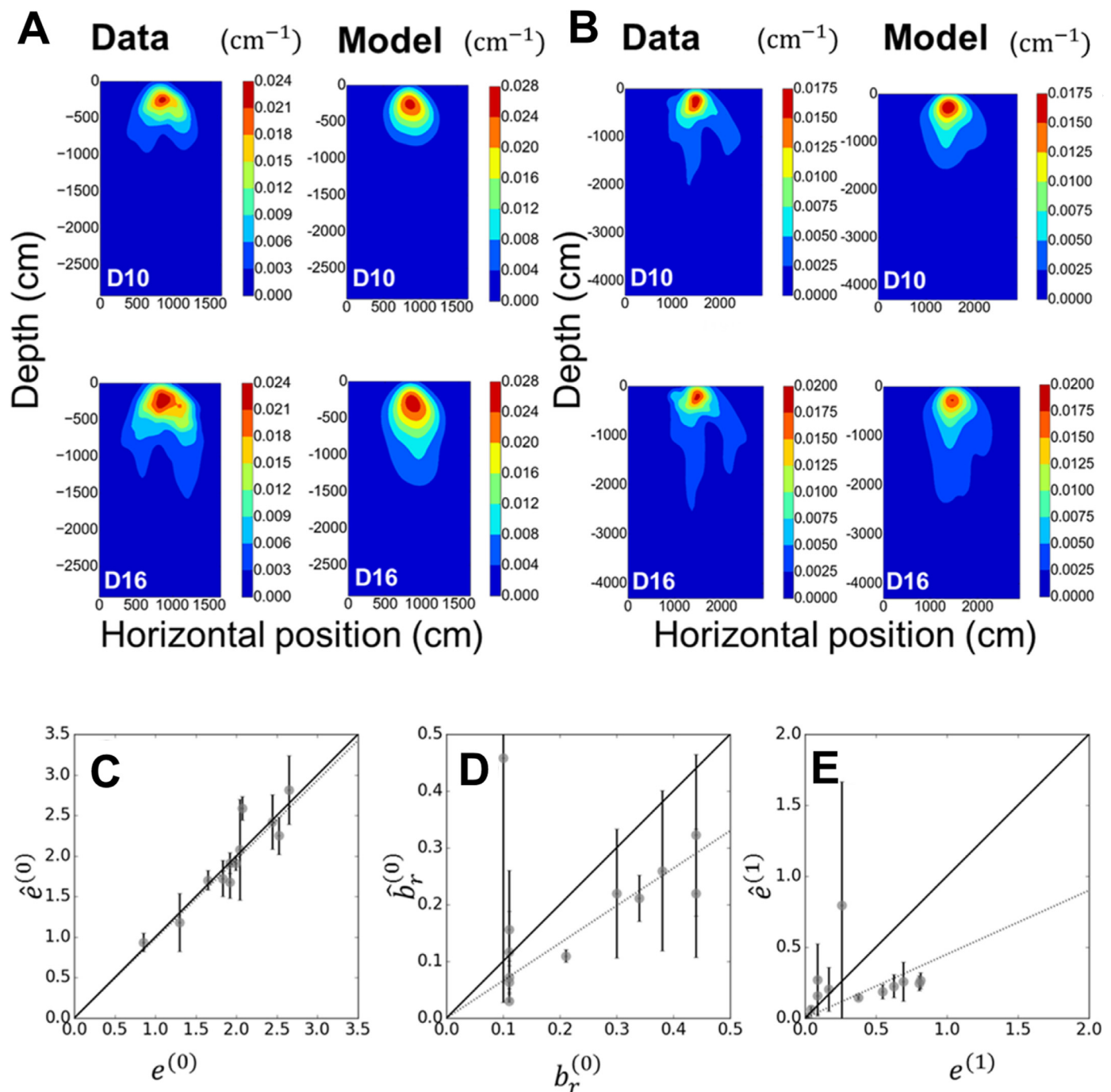


Fig. 3. Comparison between data and model predictions. After the optimisation process, root length density estimation matched the experimental data at Day 10 (D10) and Day 16 (D16) of the experiment. The data is presented for A) genotype OSU 048; and B) genotype cv. Harrington. Differences between model and data arise from the non-smooth variation in root length density due to limited number of genotypes. Overall quality of the extraction of growth parameters (C–E) was assessed by plotting the direct estimate with the model-based growth parameters for the entire dataset (all time steps and genotypes). Results show good estimation of elongation rate of primary roots $e^{(0)}$ (C) The branching rate $b_r^{(0)}$ (D) and the elongation rate $e^{(1)}$ of lateral roots (E) could also be predicted but with less accuracy due to the variability of the growth rate of lateral roots. Plain lines indicate 1:1 relations and dotted lines show differences in model predictions.

541 roots was overestimated by a factor of 1.5 (Fig. 3D). The elongation of laterals showed the weakest model predictions which were
 542 obtained with an over estimation by a factor of 2 (Fig. 3E). Likewise, the gravitropic rate was more difficult to determine exper-
 543 imentally due to the stochasticity of the direction of growth. Direct estimation of gravitropic rate was obtained using the angle of
 544 primary roots at day 2 and day 4. However, there was a strong correlation between the initial angle of the root and the magni-
 545 tude of the change in the angle ($p < 0.001$, with average R^2 of 0.59).
 546
 547
 548
 549

This confirmed the linearity of the gravitropic response as was proposed in earlier theoretical studies (Dupuy et al., 2010). However,
 550 this measure of the gravitropic rate may be of limited value because it was obtained at a fixed point in time. The measure is
 551 therefore more sensitive to root stochasticity and it may not be representative for the overall plant behaviour since the gravitropic
 552 rate may change with time. Results suggest that the global estimation of the gravitropic rate using the optimisation pipeline was
 553 more realistic (Table 1). Direct estimation of the gravitropic rate
 554
 555
 556
 557
 558

Table 1

Estimated root growth parameters for primary roots using the optimisation pipeline (Fig. 2) and comparison between measured and predicted total root length.

Genotype	Elongation (cm×d ⁻¹)		Gravitropism (d ⁻¹)		Total root length(cm)		Predicted total root length(cm)	
	Δt ₁	Δt ₂	Δt ₁	Δt ₂	Δt ₁	Δt ₂	Δt ₁	Δt ₂
OSU_048	0.85	1.30	0.258	0.224	68.30	107.42	68.91	108.72
OSU_044	1.92	1.99	0.168	0.162	109.83	164.92	110.83	166.99
Harrington	2.04	1.83	0.167	0.174	137.48	201.00	136.72	201.35
OSU_060	2.07	1.65	0.178	0.190	137.42	196.01	136.46	195.95
OSU_052	2.44	1.92	0.174	0.174	152.49	214.54	154.46	217.49
OSU_144	2.65	2.52	0.155	0.129	161.56	242.58	159.86	242.46

Table 2

Estimated root growth parameters for lateral roots using the optimisation pipeline (Fig. 2) and comparison between measured and predicted total root length.

Genotype	Branching (d ⁻¹)		Elongation (cm×d ⁻¹)		Total root length(cm)		Predicted total root length(cm)	
	Δt ₁	Δt ₂	Δt ₁	Δt ₂	Δt ₁	Δt ₂	Δt ₁	Δt ₂
OSU_048	0.383	0.109	0.690	0.260	13.52	37.27	13.42	37.05
OSU_044	0.207	0.114	0.373	0.017	3.59	4.37	7.33	8.27
Harrington	0.442	0.110	0.806	0.087	11.71	20.54	11.52	20.45
OSU_060	0.296	0.110	0.548	0.086	7.07	13.40	7.00	13.67
OSU_052	0.444	0.114	0.814	0.044	7.99	11.91	5.82	9.71
OSU_144	0.337	0.104	0.624	0.168	6.47	19.05	5.37	18.83

Table 3

Analysis of the genotype and time effect on root parameters using a mixed effect model. Statistical significance (*p*-values) are provided for the fixed effects using a chi-squared based Wald-test using residual maximum likelihood (REML). Level of significance is provided for (*) *p* < 0.05; (**) *p* < 0.01; and (***) *p* < 0.001.

Trait	Genotype	Time	Genotype × Time-step
Lateral roots number	ns	***	ns
Lateral total length	*	***	**
Log_lateral_tot_length	ns	***	*
Branching rate	ns	***	ns
Lateral elongation rate	ns	*	ns
Log_lateral_elong_rate	*	ns	**
Seminal roots number	ns	ns	ns
Seminal elongation rate	***	***	***

559 predicted genotype OSU060 to be more gravitropic than cv. Har-
 560 rington whereas they were genetically and visually very similar
 561 (Fig. 4). There was no major difference in the estimates of the grav-
 562 itropic rate obtained from the optimisation pipeline for the dura-
 563 tion of each growth period between genotypes.

564 3.3. Both genotypic and temporal factors affect root growth 565 parameters

566 Recombinant Chromosome Substitution Lines with contrasting
 567 response to drought in field trials showed remarkable genotypic
 568 variations in the morphology of their root system at early growth
 569 stages. Seminal root elongation rate was the most discriminat-
 570 ing variable across the RCSLs (*p* < 0.001, Table 3). For instance,
 571 OSU048 (stable but limited yield performance) had a remark-
 572 ably low and uniform elongation rate throughout the experiment
 573 (0.94 ± 0.04 cm d⁻¹ and 1.13 ± 0.14 cm d⁻¹ from day 2 to 10 and
 574 from day 10 to 16 respectively, Fig. 4). In contrast, OSU144 (sen-
 575 sitive but large yield potential) showed an overall decrease in
 576 elongation rate for the seminal roots, with a higher elongation
 577 rate from day 2 to 10 (2.8 ± 0.2 cm d⁻¹) than from day 10 to 16
 578 (2.3 ± 0.1 cm d⁻¹). This trend was observed for all genotypes ex-
 579 cept OSU048 and OSU044. Branching rate and lateral root elong-
 580 ation rate showed large variation at the genotype level due to
 581 the stochasticity of these growth parameters. For all the geno-

types, the number of lateral roots emerged from day 2 to day 10
 of the experiment was larger than the number of lateral roots that
 emerged from day 10 to 16. Genotypic differences were found for
 elongation rate of lateral roots (*p* < 0.05, Table 3). Lateral roots in
 OSU048 grew vigorously from day 10 to 16 (0.7 ± 0.3 cm d⁻¹) and
 this resulted in a much larger total lateral root length at the end
 of the experiment (40.2 ± 7.0 cm), compared to genotypes such as
 OSU044 (4.5 ± 1.4 cm) and OSU052 (13.3 ± 3.5 cm) which had a lat-
 eral root growth rate that was significantly lower (Fig. 4). OSU048
 and OSU144 were the two most contrasting phenotypes with a final
 total root length of 159.4 ± 10.7 cm and 284.5 ± 23.8 cm respec-
 tively. OSU060 was selected because of the similarity of its perfor-
 mance to cv. Harrington in field conditions (de La Fuente Canto,
 in preparation), and results showed its growth parameters were
 comparable to cv. Harrington (Fig. 4). This suggests the exotic in-
 trogressions present in OSU060 also had a negligible effect on the
 root system at this stage of development.

Overall, these results indicate that introgressions of exotic DNA
 in the genetic background of a modern barley can have a strong
 effect on root system architecture at establishment stage. Although
 the link between response to water deficit and root system archi-
 tecture is not demonstrated in this study, there are multiple indi-
 cations that modern agriculture and the heavy supply of water and
 fertiliser to crops have led to significant changes in the size and
 architecture of root systems (Letter et al., 2003). This was illus-
 trated in comparative studies of modern and ancient crop varieties
 (Chloupek et al., 2006). In barley, modern cultivars were found to
 have larger numbers of seminal roots with a wider angular spread
 of roots compared to their wild relatives (Bengough et al., 2004).
 To engineer crops that are efficient in low input cultivation con-
 ditions, it is probable that the roots of such new crops will need
 to acquire soil resources from different regions of the soil. For ex-
 ample, improving the rooting depth could be used for resistance to
 drought (Kato et al., 2006) and enhanced lateral root development
 in the topsoil could provide better phosphorus uptake efficiency
 (Lynch and Brown, 2002; White et al., 2013).

Although few genotypes were screened in this study, there was
 strong evidence of genotypic variations in root growth param-
 eters of the RCSL population. This result shows the potential of ex-
 otic allelic variation in the modification of root system architec-
 ture of modern barley cultivars. For example, there was significant

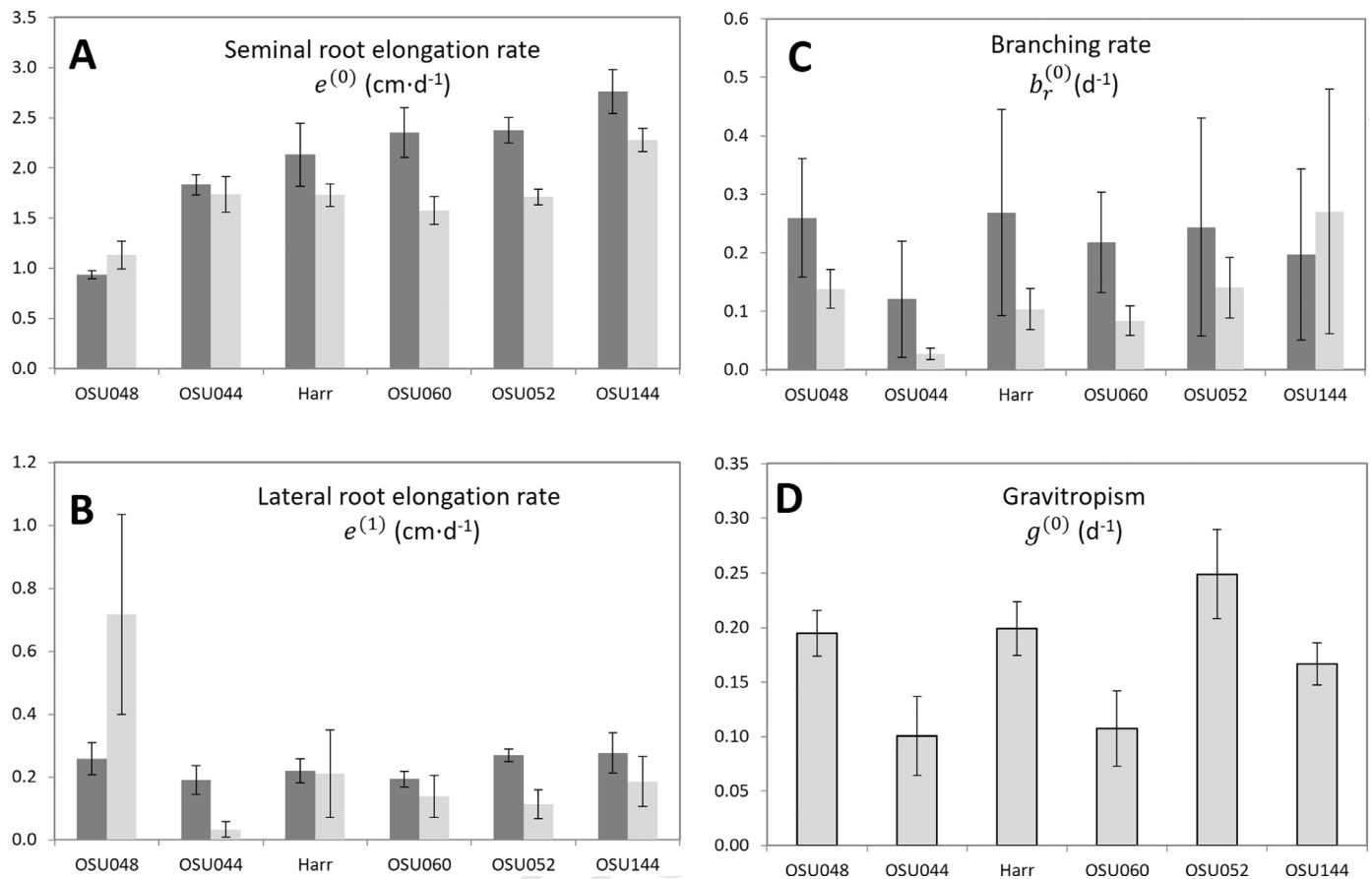


Fig. 4. Variations in root growth parameters with time and as a function of genotype. Bar charts represent mean values (\pm SE) for A) seminal root elongation rate (cm d^{-1}); B) lateral root elongation rate (cm d^{-1}); C) branching rate (d^{-1}). Growth parameters from Day 2 to Day 10 are plotted with dark grey shading, and growth parameters from Day 10 to Day 16 is plotted with light grey shading. D) Genotypes' mean value for gravitropic rate measured from Day 2 to Day 4. Error bars represent standard error of the mean.

623 variation in root gravitropism and primary root elongation rate be- 620
 624 tween the RCSL genotypes, and this could be exploited to create 621
 625 deep rooting genotypes. Del Pozo et al. (2012) found evidence sug- 622
 626 gesting segregation in the deep root phenotype within the RCSL 623
 627 population used for this study. The authors carried out a field trial 624
 628 and found that drought tolerant RCSLs had greater values of grain 625
 629 $\Delta^{13}\text{C}$ compared to cv. Harrington, which may indicate greater ac- 626
 630 cess to soil water during grain filling and a more extensive root 627
 631 system (Tambussi et al., 2007). The differences found for root elon- 628
 632 gation rate and gravitropism at early stages of development in the 629
 633 RCSLs tested in the present study support this hypothesis since 630
 634 these two traits have been associated with deep rooting phenotype 631
 635 in cereal crops (Araki et al., 2002), and they have been shown to be 632
 636 an important quantitative trait to improve water uptake and yield 633
 637 under water stress in rice (Uga et al., 2013) and maize (Hund et al., 634
 638 2009). There were also significant variations in the elongation rate 635
 639 and branching rate of lateral roots. Lateral roots are essential to the 636
 640 acquisition of nutrients because they allow intensive exploration of 637
 641 the soil between the main root axes and because of their ability to 638
 642 solubilize minerals adsorbed on the surface of soil particles. Lateral 639
 643 roots for example, have been shown to increase the uptake of im- 640
 644 mobile nutrients such as phosphorus (Lambers et al., 2006). 641

645 3.4. Analysis RCSLs phenotypic data

646 The genomes of Recombinant Chromosome Substitution Lines 642
 647 (RCSLs) are characterised by substitutions of entire blocks of the 643
 648 genome with the DNA of an ancient variety (RCSLs, Matus et al., 644
 649 2003). Because the region of DNA inserted are quite large, a much-

650 reduced number of lines is sufficient to induce variations over the 650
 651 entire genome. This is particularly appealing to root genetic stud- 651
 652 ies where phenotyping is particularly time consuming, and this 652
 653 could be used, for example, to exclude quickly regions of limited 653
 654 influence on rooting trait. However, it is unclear how best to anal- 654
 655 yse the phenotypic data of such genetic material to derived useful 655
 656 knowledge on the genetics of root growth. Traditional QTL map- 656
 657 ping analysis such as the composite interval mapping (CIM) used 657
 658 by Uga et al. (2013) in 117 rice RILs or the multiple interval map- 658
 659 ping (MIM) used by Chen et al. (2010) in a 134 F_4 barley mapping 659
 660 cannot be applied directly. 660

661 In this study, we proposed a combinatorial approach (C-QTL) to 661
 662 quantify the phenotypic effects of blocks of markers. The method 662
 663 allows visualisation of the influence of ensembles of markers that 663
 664 covary in the selection of lines employed in the study. The method 664
 665 makes group of lines and compute a score for each group of 665
 666 marker, using variations observed between and within groups. 666
 667 Since there are different ways of grouping genotypes, a cluster al- 667
 668 gorithm was used to create the sets of relevant groups on which 668
 669 the metric was cumulated. Since the metric accounts for both 669
 670 within group variability and between group variability, it empha- 670
 671 size regions of the genome that were linked to the largest varia- 671
 672 tions in a quantitative trait, but also the regions on which no in- 672
 673 formation can be derived. 673

674 The C-QTL method described here is inspired from techniques 674
 675 used in non-parametric statistics. For example, bootstrapping uses 675
 676 random resampling of the data with replacement to produce simu- 676
 677 lated data of how an estimate varies, and to compute confi- 677
 678 dence intervals of estimates directly from these simulations 678

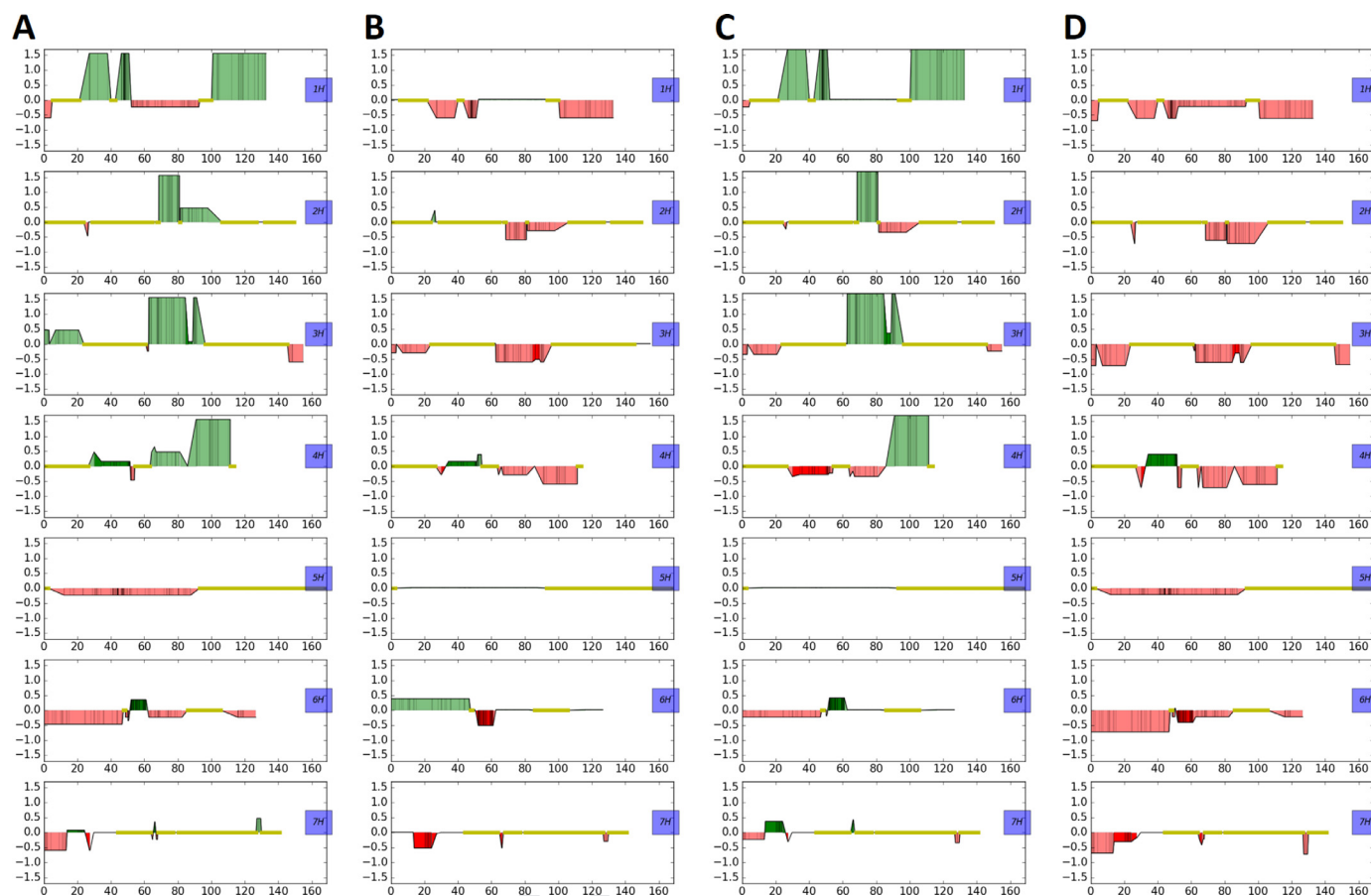


Fig. 5. Chromosome regions associated with root elongation rates. Green areas of the graph indicate region of the genome for which variations are associated with changes in the quantitative trait. Red areas of the graph indicate regions of the genome for which variations are not associated with variations in root traits. Darker regions (respectively green or red) indicate regions where there is more chromosomal introgression for which estimates are likely to be more accurate. Horizontal lines in yellow indicate region of the genome for which no genetic variations are observed within the selection of genotypes studied. Chromosome regions associated with primary elongation rate A), gravitropic rate B), lateral root elongation rate C), and branching rate D). (For interpretation of the references to colour in this figure legend, the reader is referred to the web version of this article).

679 (Efron and Tibshirani, 1994). Cross validation techniques employ
 680 a range of resampling schemes (leave-one-out, leave-p-out, V-fold,
 681 Monte Carlo) for example to determine the log likelihood of a
 682 model (Burman, 1989). In a permutation test, samples are randomly
 683 rearranged between groups to assess the likelihood of the null
 684 hypothesis (Kim et al., 2000). The method also shares some
 685 similarities with single marker mapping (Geldermann et al., 1985)
 686 since the metric determined on two sets of genotypes is a direct
 687 estimate of the effect of the group of markers that makes the two
 688 groups genetically different. However, the C-QTL approach is different
 689 from these methods, in that the whole dataset is used in the
 690 simulations and it is the grouping of the data that is resampled
 691 to compute the net effect of a marker. Intuitively, the method provides
 692 an optimal way of grouping genotypes that minimises the number of
 693 computations while maximises the information contained in the metric.

695 The method was tested on a larger selection of RCSL lines using
 696 heading date as a reference trait and results can be access on Zenodo
 697 repository (de la Fuede Canto, 2018). The test showed C-QTL co-locate
 698 with key genomic regions associated with barley phenology (de la Fuede
 699 Canto, 2016). To date, however, it is unclear how the resampling of the
 700 groups affects the bias and variance of the estimators of the marker
 701 effect, and how different ways of grouping genotypes could improve
 702 the quality of the estimates. Additional theoretical work is now required
 703 to further characterise the mathematical properties of C-QTL estimates.
 704 Further development could also expand the technique to include common
 705 statistics on

the significance of the effects of markers. For example, permutation
 706 tests could be implemented in the C-QTL analysis to determine the
 707 statistical significance of the QTLs identified (Doerge and Churchill,
 708 1996), because they do not require *a priori* knowledge of the
 709 statistical distribution of the sample data.

711 C-QTL analysis provided a coarse but extensive map of the influence
 712 of wild barley chromosomal introgression on rooting traits (Figs. 5 and 6).
 713 Because of the small number of genotypes studied, only a few substitution
 714 segments from the wild genome were tested and associations for several
 715 root growth parameters are likely to co-vary with other unrelated markers
 716 (Fig. 1D). Regions associated with primary and lateral root elongation
 717 rates (Fig. 5A, C) were mostly identical across the genome, with the
 718 highest scores recorded simultaneously on chromosomes 1H, 2H, 3H and
 719 4H, moderate score values on chromosome 6H and no associations on
 720 chromosome 5H. In addition, small groups of markers on chromosomes
 721 2H, 3H, and 7H appear to be solely associated with the elongation rate
 722 of seminal roots whereas a common group of markers on chromosome
 723 4H was found to overlap with seminal elongation rate, gravitropism and
 724 branching rate. In particular, the wild barley introgression on
 725 chromosome 2H (68.6cM to 80.9cM) found on OSU048 could be linked
 726 in elongation rate. Few QTLs have been reported in the literature for
 727 root growth rate parameters in barley (Gregory et al., 2009), while
 728 Chen et al. (2010) and (Arifuzzaman et al., 2014) detected genomic
 729 regions on chromosomes 2H, 3H and 5H influencing root length. Both
 730 authors used populations derived from Israeli wild barley accessions in
 731 their

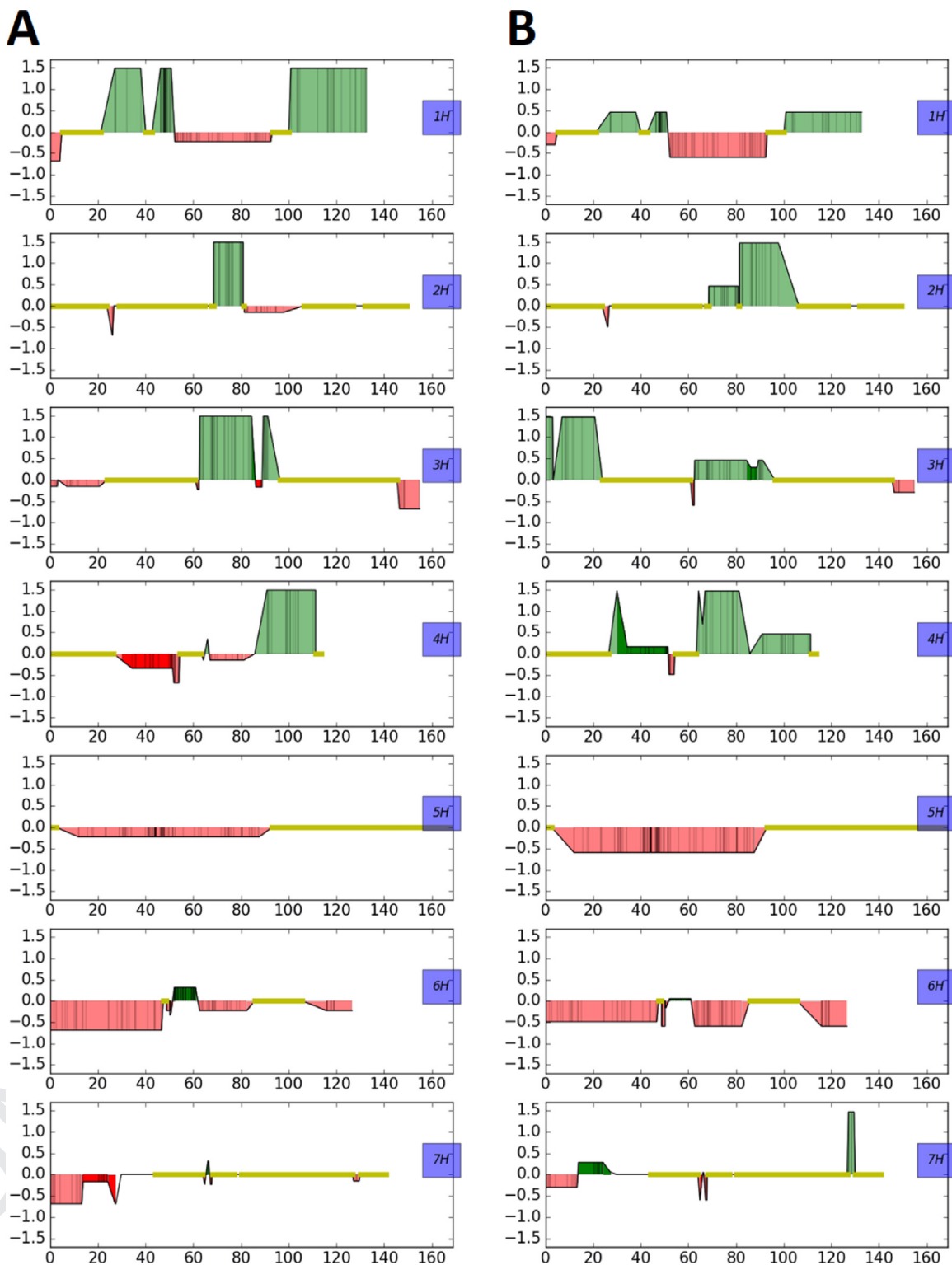


Fig. 6. Change in regions associated with primary elongation rate with time. Chromosome regions associated with primary elongation rate at day 10 A) and primary elongation rate at day 16 B) showed a few differences in chromosomes 2H, 3H, 4H and 7H.

733 studies and showed the potential of the unadapted genome to con-
 734 tribute favourable alleles to increase root length and subsequent
 735 adaptation to water-limited environments.

736 Regions associated with gravitropic rate (Fig. 5B) and branch-
 737 ing rate (Fig. 5D) were less significant than the associations found
 738 for elongation rate of primary and lateral roots. Two regions on
 739 chromosome 2H and 6H were uniquely associated with gravitropic

rate and a large group of markers chromosome 5H was found to
 be associated with the trait but with a very low score. Recently
 Robinson et al. (2016) reported a major QTL associated with
 root spread on chromosome 5H using a double haploid popula-
 tion (ND24260 X Flagship). The authors found this region col-
 located with other QTL controlling seminal root number which also
 mapped in the vicinity of aboveground quantitative traits related

747 to drought adaptation in barley. A chromosomal region on 7H was
748 associated solely with the elongation rate of lateral roots and a
749 chromosomal region on 4H was associated only with the branching
750 rate. No QTLs have been reported for this trait in previous studies.
751 It is also interesting to note that the score of markers associated
752 with the primary elongation rate and the branching rate varied
753 strongly as a function of time (Fig. 6), whereas the score associ-
754 ated with the elongation rate of lateral roots was more consistent
755 at the different time steps.

756 Accurate identification of root QTL from a small subset of RCSL
757 genotypes is challenging. First results showed correlations exist be-
758 tween groups of markers because of limited number of genotypic
759 combinations within the genome (Fig. 1). Physiological interactions
760 are also likely to create natural correlations between several traits.
761 It is often observed that elongation of primary and lateral roots
762 are linked; for example, enhanced elongation of lateral roots coin-
763 cides with a reduction in the growth of primary (Williamson et al.,
764 2001). In order to overcome such limitations, it is important there-
765 fore, to optimise the distribution of wild introgressions within a
766 selection of RCSL genotypes to be used in a study. An essential
767 property to consider for the C-QTL approach is the balance be-
768 tween wild and cultivated introgressions within the selection of
769 genotypes. An ideal set of lines would have introgressions arranged
770 with minimum overlapping of segments and each marker would
771 appear in exactly the same number of times in the set of geno-
772 types. This is difficult to achieve practically because of the large
773 number of genotypes that would be required. For example, with 10
774 segments a full factorial set of introgressions would require 210–
775 1024 genotypes. A more straightforward and effective approach
776 would be to phenotype introgression lines harbouring a unique ex-
777 otic insert from the donor parent genome. Lines from the initial
778 cross between cv. Scarlett X ISR42-8 (Von Korff et al., 2004) have
779 been further backcrossed to the recurrent parent and new subsets
780 of lines with unique introgressions have been used in root QTL
781 mapping studies (Hoffmann et al., 2012; Naz et al., 2014). In this
782 case, QTLs are located to the target segment making the introgres-
783 sion line significantly different from the donor parent and the re-
784 sults can be validated using a small number of introgression lines
785 (Ahmad Naz et al., 2012). However, this approach is not suitable for
786 groups of introgression lines in earlier generations (BC2) since they
787 contain several alien inserts in their genome. The C-QTL approach
788 could aid the selection of target regions putatively associated with
789 the trait for further experiments, optimising the number of intro-
790 gression lines used and the backcross strategy to obtain near iso-
791 genic lines and ultimately identify the genes underlying the QTL.

792 4. Conclusion

793 The speed and efficiency of root phenotyping is limiting the
794 ability of research groups to map QTLs of root-related traits. The
795 combined imaging and modelling pipeline developed in this paper
796 allowed efficient measurement of root traits and potential identifi-
797 cation of QTLs linked to root elongation, branching rate and grav-
798 itropism for both main axes and first order lateral roots in barley.
799 The use of barley RCSLs with well-defined chromosomal introgres-
800 sions enabled identification of QTLs of interest with relatively few
801 lines in a time lapse dataset. The immediate next step is to design
802 the next generation of RCSL lines and so better refine the chromo-
803 somal regions associated with root growth parameters. This gener-
804 al approach should be transportable between crop species and
805 may be applicable in a wider range of growth systems where roots
806 can be imaged, including root boxes where roots are grown in
807 soil. As such, the proposed framework is a valuable step forward
808 in advancing the range of methods available for root phenotyping,
809 though further testing and verification will be needed for each new
810 crop growth system adopted.

Acknowledgement

Michael Adu provided invaluable help during the development
of the experimental set up. We also thank Prof. X. Draye for use-
ful discussions during the design of this work and Philip White
for the valuable comments provided on the manuscript. This work
was supported by the EU FP7 project EUroot 'Enhanced models for
predicting RSA development under multiple 'stresses' (2011–2016,
KBBE.2011.1.2-05 no. 289300). The James Hutton Institute received
support from the Scottish Government Rural and Environment Sci-
ence and Analytical Services Division (RESAS, Workpackage 2.1.7,
2.3.4)

References

- Adu, M.O., Chatot, A., Wiesel, L., Bennett, M.J., Broadley, M.R., White, P.J., Dupuy, L.X.,
2014. A scanner system for high-resolution quantification of variation in root
growth dynamics of *Brassica rapa* genotypes. *J. Exp. Bot.* 54, 1431–1446. doi:10.
1093/jxb/eru048.
- Ahmad Naz, A., Ehl, A., Pillen, K., Léon, J., 2012. Validation for root related quan-
titative trait locus effects of wild origin in the cultivated background of barley
(*Hordeum vulgare* L.). *Plant Breed.* 131, 392–398.
- Arai-Sanoh, Y., Takai, T., Yoshinaga, S., Nakano, H., Kojima, M., Sakakibara, H.,
Kondo, M., Uga, Y., 2014. Deep rooting conferred by deeper rooting 1 enhances
rice yield in paddy fields. *Sci. Rep.* 4.
- Araki, H., Morita, S., Tatsumi, J., Iijima, M., 2002. Physiol-morphological analysis on
axile root growth in upland rice. *Plant Prod. Sci.* 5, 286–293.
- Arifuzzaman, M., Sayed, M.A., Muzammil, S., Pillen, K., Schumann, H., Naz, A.A.,
Léon, J., 2014. Detection and validation of novel QTL for shoot and root traits
in barley (*Hordeum vulgare* L.). *Mol. Breed.* 34, 1373–1387.
- Armengaud, P., Zambaux, K., Hills, A., Sulpice, R., Pattison, R.J., Blatt, M.R., Amt-
mann, A., 2009. EZ-Rhizo: integrated software for the fast and accurate mea-
surement of root system architecture. *Plant J.* 57, 945–956.
- Atkinson, J.A., Wingen, L.U., Griffiths, M., Pound, M.P., Gaju, O., Foulkes, M.J., Le
Gouis, J., Griffiths, S., Bennett, M.J., King, J., 2015. Phenotyping pipeline reveals
major seedling root growth QTL in hexaploid wheat. *J. Exp. Bot.* 66, 2281–2292.
- Bengough, A.G., Gordon, D.C., Al-Menaie, H., Ellis, R.P., Allan, D., Keith, R.,
Thomas, W.T.B., Forster, B.P., 2004. Gel observation chamber for rapid screen-
ing of root traits in cereal seedlings. *Plant Soil* 262, 63–70.
- Bingham, I.J., Bengough, A.G., Rees, R.M., 2010. Soil compaction–N interactions in
barley: root growth and tissue composition. *Soil Tillage Res.* 106, 241–246.
- Boserup, E., 2005. The Conditions of Agricultural Growth: The economics of Agrarian
Change under Population Pressure. Transaction Publishers.
- Burman, P., 1989. A comparative study of ordinary cross-validation, v-fold cross-
validation and the repeated learning-testing methods. *Biometrika* 76, 503–514.
- Cai, G., Vanderborcht, J., Klotzsch, A., van der Kruk, J., Neumann, J., Hermes, N.,
Vereecken, H., 2016. Construction of minirhizotron facilities for investigating
root zone processes. *Vadose Zone J.* 15.
- Chen, G., Krugman, T., Fahima, T., Chen, K., Hu, Y., Röder, M., Nevo, E., Korol, A., 2010.
Chromosomal regions controlling seedling drought resistance in Israeli wild bar-
ley, *Hordeum spontaneum* C. Koch. *Genet Resour Crop Evol* 57, 85–99.
- Chloupek, O., Forster, B.P., Thomas, W.T., 2006. The effect of semi-dwarf genes on
root system size in field-grown barley. *Theor Appl Genet* 112, 779–786.
- Clark, R.T., MacCurdy, R.B., Jung, J.K., Shaff, J.E., McCouch, S.R., Aneshansley, D.J.,
Kochian, L.V., 2011. Three-dimensional root phenotyping with a novel imaging
and software platform. *Plant Physiol.* 156, 455–465.
- Comas, L., Becker, S., Cruz, V.M.V., Byrne, P.F., Dierig, D.A., 2013. Root traits con-
tributing to plant productivity under drought. *Front. Plant Sci.* 4. doi:10.3389/
fpsl.2013.00442.
- Courtois, B., Ahmadi, N., Khowaja, F., Price, A.H., Rami, J.-F., Frouin, J., Hamelin, C.,
Ruiz, M., 2009. Rice root genetic architecture: meta-analysis from a drought QTL
database. *Rice* 2, 115–128.
- de Dorlodot, S., Forster, B., Pagès, L., Price, A., Tuberoso, R., Draye, X., 2007. Root
system architecture: opportunities and constraints for genetic improvement of
crops. *Trends Plant Sci.* 12, 474–481.
- de la Fuede Canto, C. (2016). Recombinant Chromosome Substitution Lines as a
source of genetic variation for drought stress tolerance in barley Vol. PhD. Uni-
versity of Dundee.
- de la Fuede Canto, C. (2018). Test data for C-QTL analysis of barley recombinant
chromosome substitution lines. <https://doi.org/10.5281/zenodo.1196298>.
- Del Pozo, A., Castillo, D., Inostroza, L., Matus, I., Méndez, A., Morcuende, R., 2012.
Physiological and yield responses of recombinant chromosome substitution
lines of barley to terminal drought in a Mediterranean type environment. *Ann.
Appl. Biol.* 160, 157–167.
- do Rosario, M., Oliveira, G., Van Noordwijk, M., Gaze, S.R., Brouwer, G., Bona, S.,
Mosca, G., Hairiah, K., et al., 2000. Auger sampling, ingrowth cores and pinboard
methods. In: Smit, A., et al. (Eds.), *Root Method a Handbook*. Springer, Berlin.
- Doerge, R.W., Churchill, G.A., 1996. Permutation tests for multiple loci affecting a
quantitative character. *Genetics* 142, 285–294.
- Downie, H., Holden, N., Otten, W., Spiers, A.J., Valentine, T.A., Dupuy, L.X., 2012.
Transparent soil for imaging the rhizosphere. *PLoS One* 7, e44276.

- 889 Downie, H., Adu, M., Schmidt, S., Otten, W., Dupuy, L., White, P., Valentine, T., 2015. Challenges and opportunities for quantifying roots and rhizosphere interactions through imaging and image analysis. *Plant, Cell Environ.* 38, 1213–1232.
- 890 Dupuy, L.X., Vignes, M., McKenzie, B., White, P., 2010. The dynamics of root meristem distribution in soil. *Plant, Cell Environ.* 33, 358–369.
- 891 Efron, B., Tibshirani, R.J., 1994. *An Introduction to the Bootstrap*. CRC press.
- 892 Forde, B., Lorenzo, H., 2001. The nutritional control of root development. *Plant Soil* 232, 51–68.
- 893 Forde, B.G., 2009. Is it good noise? The role of developmental instability in the shaping of a root system. *J. Exp. Bot.* 60, 3989–4002.
- 894 Garré, S., Laloy, E., Javaux, M., Vereecken, H., 2012. Parameterizing a dynamic architectural model of the root system of spring barley from minirhizotron data. *Vadose Zone J.* 11.
- 895 Geldermann, H., Pieper, U., Roth, B., 1985. Effects of marked chromosome sections on milk performance in cattle. *Theor. Appl. Genet.* 70, 138–146.
- 896 Gioia, T., Galinski, A., Lenz, H., Müller, C., Lentz, J., Heinz, K., Briese, C., Putz, A., Fiorani, F., Watt, M., 2017. GrowScreen-PaGe, a non-invasive, high-throughput phenotyping system based on germination paper to quantify crop phenotypic diversity and plasticity of root traits under varying nutrient supply. *Funct. Plant Biol.* 44, 76–93.
- 897 Gregory, P.J., Bengough, A.G., Grinev, D., Schmidt, S., Thomas, W.T.B., Wojciechowski, T., Young, I.M., 2009. Root phenomics of crops: opportunities and challenges. *Funct. Plant Biol.* 36, 922–929. doi:10.1071/FP09150.
- 898 Hackett, C., Rose, D., 1972. A model of the extension and branching of a seminal root of barley, and its use in studying relations between root dimensions. 1. The model. *Aust. J. Biol. Sci.* 25, 669–679.
- 899 Heinen, M., Mollier, A., De Willigen, P., 2003. Growth of a root system described as diffusion. 2. Numerical model and application. *Plant Soil* 252, 251–265.
- 900 Hoffmann, A., Maurer, A., Pillen, K., 2012. Detection of nitrogen deficiency QTL in juvenile wild barley introgression lines growing in a hydroponic system. *BMC Genet.* 13, 88.
- 901 Hund, A., Ruta, N., Liedgens, M., 2009. Rooting depth and water use efficiency of tropical maize inbred lines, differing in drought tolerance. *Plant Soil* 318, 311–325.
- 902 Kalogiros, D.I., Adu, M.O., White, P.J., Broadley, M.R., Draye, X., Ptashnyk, M., Bengough, A.G., Dupuy, L.X., 2016. Analysis of root growth from a phenotyping data set using a density-based model. *J. Exp. Bot.* 67, 1045–1058. doi:10.1093/jxb/erv573.
- 903 Kato, Y., Abe, J., Kamoshita, A., Yamagishi, J., 2006. Genotypic variation in root growth angle in rice (*Oryza sativa* L.) and its association with deep root development in upland fields with different water regimes. *Plant Soil* 287, 117–129.
- 904 Kim, H.J., Fay, M.P., Feuer, E.J., Midthune, D.N., 2000. Permutation tests for jointpoint regression with applications to cancer rates. *Stat. Med.* 19, 335–351.
- 905 Kristensen, H.L., Thorup-Kristensen, K., 2004. Root growth and nitrate uptake of three different catch crops in deep soil layers. *Soil Sci. Soc. Am. J.* 68, 529–537.
- 906 Kumar, P., Huang, C., Cai, J., Miklavic, S.J., 2014. Root phenotyping by root tip detection and classification through statistical learning. *Plant Soil* 380, 193–209.
- 907 Lambers, H., Shane, M.W., Cramer, M.D., Pearce, S.J., Veneklaas, E.J., 2006. Root structure and functioning for efficient acquisition of phosphorus: Matching morphological and physiological traits. *Ann. Bot.* 98, 693–713.
- 908 Le Marié, C., Kirchgessner, N., Marschall, D., Walter, A., Hund, A., 2014. Rhizoslides: paper-based growth system for non-destructive, high throughput phenotyping of root development by means of image analysis. *Plant Methods* 10, 1.
- 909 Leitner, D., Felderer, B., Vontobel, P., Schnepf, A., 2014. Recovering root system traits using image analysis exemplified by two-dimensional neutron radiography images of lupine. *Plant Physiol.* 164, 24–35.
- 910 Letter, D., Seidel, R., Liebhardt, W., 2003. The performance of organic and conventional cropping systems in an extreme climate year. *Am. J. Altern. Agric.* 18, 146–154.
- 911 Liao, H., Rubio, G., Yan, X., Cao, A., Brown, K.M., Lynch, J.P., 2001. Effect of phosphorus availability on basal root shallowness in common bean. *Plant Soil* 232, 69–79.
- 912 Lobet, G., Pagès, L., Draye, X., 2011. A novel image-analysis toolbox enabling quantitative analysis of root system architecture. *Plant Physiol.* 157, 29–39.
- 913 Lynch, J., Brown, K., 2002. Topsoil foraging - an architectural adaptation of plants to low phosphorus availability. *Plant Soil* 237, 225–237.
- 914 Lynch, J.P., 2011. Root phenes for enhanced soil exploration and phosphorus acquisition: Tools for future crops. *Plant Physiol.* 156, 1041–1049. doi:10.1104/pp.111.175414.
- 915 Mairhofer, S., Zappala, S., Tracy, S.R., Sturrock, C., Bennett, M., Mooney, S.J., Pridmore, T., 2012. RooTrak: automated recovery of three-dimensional plant root architecture in soil from X-ray microcomputed tomography images using visual tracking. *Plant Physiol.* 158, 561–569.
- 916 Makowski, P., Sorensen, T.S., Therkildsen, S.V., Materka, A., Stodkilde-Jørgensen, H., Pedersen, E.M., 2002. Two-phase active contour method for semiautomatic segmentation of the heart and blood vessels from MRI images for 3D visualization. *Comput. Med. Imaging Graph.* 26, 9–17.
- 917 Matus, I., Corey, A., Filichkin, T., Hayes, P., Vales, M., Kling, J., Riera-Lizarazu, O., Sato, K., Powell, W., Waugh, R., 2003. Development and characterization of recombinant chromosome substitution lines (RCSLs) using *Hordeum vulgare* subsp. spontaneum as a source of donor alleles in a *Hordeum vulgare* subsp. vulgare background. *Genome* 46, 1010–1023.
- 918 Mooney, S., Pridmore, T., Helliwell, J., Bennett, M., 2012. Developing X-ray computed tomography to non-invasively image 3-D root systems architecture in soil. *Plant Soil* 352, 1–22.
- 919 Nagel, K.A., Putz, A., Gilmer, F., Heinz, K., Fischbach, A., Pfeifer, J., Faget, M., Blossfeld, S., Ernst, M., Dimaki, C., 2012. GROWSCREEN-Rhizo is a novel phenotyping robot enabling simultaneous measurements of root and shoot growth for plants grown in soil-filled rhizotrons. *Funct. Plant Biol.* 39, 891–904.
- 920 Naz, A.A., Arifuzzaman, M., Muzammil, S., Pillen, K., Léon, J., 2014. Wild barley introgression lines revealed novel QTL alleles for root and related shoot traits in the cultivated barley (*Hordeum vulgare* L.). *BMC Genet.* 15, 107.
- 921 Pedregosa, F., Varoquaux, G., Gramfort, A., Michel, V., Thirion, B., Grisel, O., Blondel, M., Prettenhofer, P., Weiss, R., Dubourg, V., 2011. Scikit-learn: machine learning in Python. *J. Mach. Learn. Res.* 12, 2825–2830.
- 922 Pound, M.P., French, A.P., Atkinson, J.A., Wells, D.M., Bennett, M.J., Pridmore, T., 2013. RootNav: navigating images of complex root architectures. *Plant Physiol.* 162, 1802–1814.
- 923 Reddy, V.R., Pachepsky, Y.A., 2001. Testing a convective-dispersive model of two-dimensional root growth and proliferation in a greenhouse experiment with maize plants. *Ann. Bot.* 87, 759–768.
- 924 Rewald, B., Ephrath, J.E., 2012. *Minirhizotron Technique*. Plant Roots: The Hidden Half, 4th edn CRC Press, New York.
- 925 Robinson, H., Hickey, L., Richard, C., Mace, E., Kelly, A., Borrell, A., Franckowiak, J., & Fox, G. (2016). Genomic regions influencing seminal root traits in barley. *The Plant Genome* 9.
- 926 Rose, D., 1983. The description of the growth of root systems. *Plant Soil* 75, 405–415.
- 927 Sandhu, N., Kumar, A., 2017. Bridging the rice yield gaps under Drought: QTLs, genes, and their use in breeding programs. *Agronomy* 7, 27.
- 928 Schindelin, J., Arganda-Carreras, I., Frise, E., Kaynig, V., Longair, M., Pietzsch, T., Preibisch, S., Rueden, C., Saalfeld, S., Schmid, B., 2012. Fiji: an open-source platform for biological-image analysis. *Nat. Methods* 9, 676–682.
- 929 Secchi, S., Gassman, P.W., Jha, M., Kurkalova, L., Feng, H.H., Campbell, T., Kling, C.L., 2007. The cost of cleaner water: assessing agricultural pollution reduction at the watershed scale. *J. Soil Water Conserv.* 62, 10–21.
- 930 Shelden, M.C., Roessner, U., Sharp, R.E., Tester, M., Bacic, A., 2013. Genetic variation in the root growth response of barley genotypes to salinity stress. *Funct. Plant Biol.* 40, 516–530.
- 931 Tambussi, E., Bort, J., Araus, J., 2007. Water use efficiency in C3 cereals under Mediterranean conditions: a review of physiological aspects. *Ann. Appl. Biol.* 150, 307–321.
- 932 Thomas, C., Graham, N., Hayden, R., Meacham, M., Neugebauer, K., Nightingale, M., Dupuy, L., Hammond, J., White, P., Broadley, M., 2016. High-throughput phenotyping (HTP) identifies seedling root traits linked to variation in seed yield and nutrient capture in field-grown oilseed rape (*Brassica napus* L.). *Ann. Bot.* 118, 655–665.
- 933 Topp, C.N., Iyer-Pascuzzi, A.S., Anderson, J.T., Lee, C.-R., Zurek, P.R., Symonova, O., Zheng, Y., Bucksch, A., Mileyko, Y., Galkovskiy, T., 2013. 3D phenotyping and quantitative trait locus mapping identify core regions of the rice genome controlling root architecture. *Proc. Natl. Acad. Sci.* 110, E1695–E1704.
- 934 Trachsel, S., Kaeppler, S.M., Brown, K.M., Lynch, J.P., 2011. Shovelomics: high throughput phenotyping of maize (*Zea mays* L.) root architecture in the field. *Plant Soil* 341, 75–87.
- 935 Uga, Y., Sugimoto, K., Ogawa, S., Rane, J., Ishitani, M., Hara, N., Kitomi, Y., Inukai, Y., Ono, K., Kanno, N., 2013. Control of root system architecture by DEEPER ROOTING 1 increases rice yield under drought conditions. *Nat. Genet.* 45, 1097–1102.
- 936 Valentine, T.A., Hallett, P.D., Binnie, K., Young, M.W., Squire, G.R., Hawes, C., Bengough, A.G., 2012. Soil strength and macropore volume limit root elongation rates in many UK agricultural soils. *Ann. Bot.* 110, 259–270. doi:10.1093/aob/mcs118.
- 937 Von Korff, M., Wang, H., Léon, J., Pillen, K., 2004. Development of candidate introgression lines using an exotic barley accession (*Hordeum vulgare* ssp. spontaneum) as donor. *Theor. Appl. Genet.* 109, 1736–1745.
- 938 Watt, M., Kirkegaard, J.A., Rebetzke, G.J., 2005. A wheat genotype developed for rapid leaf growth copes well with the physical and biological constraints of unploughed soil. *Funct. Plant Biol.* 32, 695–706.
- 939 White, P.J., Broadley, M.R., Gregory, P.J., 2012. Managing the nutrition of plants and people. *Appl. Environ. Soil Sci.* 2012, 104826.
- 940 White, P.J., George, T.S., Gregory, P.J., Bengough, A.G., Hallett, P.D., McKenzie, B.M., 2013. Matching roots to their environment. *Ann. Bot.* 112, 207–222.
- 941 Wilkinson, S., Davies, W.J., 2002. ABA-based chemical signalling: the co-ordination of responses to stress in plants. *Plant Cell Environ.* 25, 195–210.
- 942 Williamson, L.C., Ribrioux, S.P., Fitter, A.H., Leyser, H.O., 2001. Phosphate availability regulates root system architecture in Arabidopsis. *Plant Physiol.* 126, 875–882.